The dynamics of starvation and recovery

Justin D. Yeakel,[1, 2, 3, 4] Christopher P. Kempes,[2, 3] and Sidney Redner[2, 3]

[1] *School of Natural Sciences, University of California, Merced, Merced, CA 95340, USA*

[2] *The Santa Fe Institute, 1399 Hyde Park Road, Santa Fe, NM 87501, USA*

[3] *Contributed equally*

[4] *Corresponding author: jdyeakel@gmail.com*

The eco-evolutionary dynamics of species are fundamentally linked to the energetic constraints of its constituent individuals. Of particular importance is the interplay between reproduction and the dynamics of starvation and recovery. We introduce a minimal nutritional state-structured model that incorporates two classes of consumer: nutritionally replete, reproducing consumers, and undernourished, non-reproducing consumers. We obtain strong constraints on starvation and recovery rates by deriving allometric scaling relationships and find that population dynamics are typically driven to a steady state. Moreover, we find that these rates fall within a 'refuge' in parameter space, where the probability of extinction of the consumer population is minimized. We also show that our model provides a natural framework that predicts maximum body size for mammals by determining the relative stability of an otherwise homogeneous population to a competing population with altered percent body fat, providing a principled mechanism for a within-lineage driver of Cope's rule.

The behavioral ecology of all organisms is influenced by the energetic state of individuals, which directly influences how they invest reserves in uncertain environments. Such behaviors are generally manifested as tradeoffs between investing in somatic maintenance and growth, or allocating energy towards reproduction[1–3]. The timing of these behaviors responds to selective pressure, as the choice of the investment impacts future fitness[4–6]. The influence of resource limitation on an organism's ability to maintain its nutritional stores may lead to repeated delays or shifts in reproduction over the course of an organism's life.

The balance between (a) somatic growth and maintenance, and (b) reproduction depends on resource availability[7]. For example, reindeer invest less in calves born after harsh winters (when the mother's energetic state is depleted) than in calves born after moderate winters[8]. Many bird species invest differently in broods during periods of resource scarcity compared to normal periods[9,10], sometimes delaying or even foregoing reproduction for a breeding season[1,11,12]. Even freshwater and marine zooplankton have been observed to avoid reproduction under nutritional stress[13], and those that do reproduce have lower survival rates[2]. Organisms may also separate maintenance and growth from reproduction over space and time: many salmonids, birds, and some mammals return to migratory breeding grounds to reproduce after one or multiple seasons in resource-rich environments where they accumulate reserves[14–16].

Physiology also plays an important role in regulating reproductive expenditures during periods of resource limitation. Many mammals (47 species in 10 families) exhibit delayed implantation, whereby females postpone fetal development until nutritional reserves can be accumulated[17,18]. Many other species (including humans) suffer irregular menstrual cycling and higher abortion rates during periods of nutritional stress[19,20]. In the extreme case of unicellular organisms, nutrition directly controls growth to a reproductive state[3,21]. The existence of so many independently evolved mechanisms across such a diverse suite of organisms highlights the universality of the fundamental tradeoff between somatic and reproductive investment.

Including individual energetic dynamics[22] in a population-level framework[22,23] is challenging[24], and a common simplifying approach is provided in the classic Lotka-Volterra (LV) model, which assumes that consumer population growth rate depends linearly on resource density[25]. Here, we introduce an alternative approach—the Nutritional State-structured Model (NSM)—that accounts for resource limitation through the consequences of starvation. In contrast to the LV model, the NSM incorporates two consumer states: hungry and full, with only the former susceptible to mortality and only the latter possessing sufficient energetic reserves to reproduce. Additionally, we incorporate allometrically derived constraints on reproduction[3], incorporating the timescales of starvation and recovery. As we shall show, our model makes several important predictions: (i) the dynamics are typically driven to a refuge far from cyclic behavior and extinction risk, (ii) steady state conditions of the NSM accurately predict measured biomass densities for mammals as well as Damuth's energetic equivalence principle, (iii) an allometrically constrained upper-bound for mammalian body size, and (iv) a selective mechanism for the evolution of larger body size, known as Cope's rule.

Nutritional state-structured model (NSM). We begin by defining a minimal Nutritional State-structured population Model (NSM), where the consumer population is partitioned into two states: (a) an energetically replete (full) state F, where the consumer reproduces at a constant rate λ and does not die from starvation, and (b) an energetically deficient (hungry) state H, where the consumer does not reproduce but dies by starvation at rate μ. The dynamics of the underlying re-
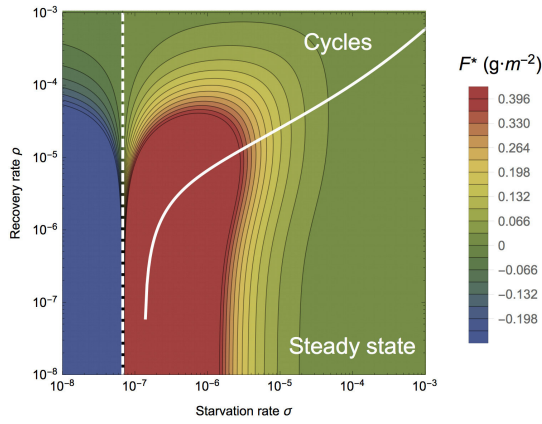
Figure 1: The transcritical (TC; dashed line) and Hopf bifurcation (solid line) as a function of the starvation rate σ and recovery rate ρ for a 100g consumer. These bifurcation conditions separate parameter space into unphysical (left of the TC), cyclic, and steady state dynamic regimes. The colors show the steady state densities for the energetically replete consumers F^*.

source R is governed by logistic growth with an intrinsic growth rate α and a carrying capacity C. The rate at which consumers transition between states and consume resources is dependent on their number, the abundance of resources, the efficiency of converting resources into metabolism, and how that metabolism is partitioned between maintenance and growth purposes. We provide a physiologically and energetically mechanistic model for each of these dynamics and constants (see the Supplementary Information (SI)), and show that the system produces a simple non-dimensional form which we describe below.

Consumers transition from the full state F to the hungry state H at a rate σ—the starvation rate—and also in proportion to the absence of resources $(1 - R)$ (we assume a maximum density, the carrying capacity equal to 1). Conversely, consumers recover from state H to state F at rate $\xi\rho$ and in proportion to R, where ξ represents a ratio between maximal resource consumption and the carrying capacity of the resource. The resources that are eaten by hungry consumers (at rate $\rho R + \delta$) account for their somatic growth (ρR) and maintenance (δ). Full consumers eat resources at a constant rate β that accounts for maximal maintenance and somatic growth (see the SI for mechanistic derivations of these rates from resource energetics). The NSM represents an ecologically motivated fundamental extension of the idealized starving random walk model of foraging, which focuses on resource depletion, to include reproduction and resource replenishment[26–28], and is a more general formulation than previous models incorporating starvation[29].

In the mean-field approximation, in which the consumers and resources are perfectly mixed, their densities are governed by the rate equations

$$\dot{F} = \lambda F + \xi\rho RH - \sigma\left(1 - R\right)F,$$
$$\dot{H} = \sigma\left(1 - R\right)F - \xi\rho RH - \mu H, \qquad (1)$$
$$\dot{R} = \alpha\left(1 - R\right)R - \left(\rho R + \delta\right)H - \beta F$$

This system of nondimensional equations follows from a set of first-principle relationships for resource consumption and growth (see the SI for a full derivation and the dimensional form). Notice that the total consumer density $F + H$ evolves according to $\dot{F} + \dot{H} = \lambda F - \mu H$. This resembles the equation of motion for the predator density in the LV model[30], except that the resource density does not appear in the growth term. The rate of reproduction is independent of resource density because it is assumed that the satiated state of the full consumer allows it to partition a constant amount of energy towards reproduction, whereas a starved consumer partitions no energy towards reproduction. The rate of reproduction for the total consumer density *is* dependent on resource density, which determines the size of the full and starved portions of the consumer population. Similarly, the consumer maintenance terms (δH and βF) are independent of resource density because they represent a minimal energetic requirement for consumers in the H and F state, respectively. It follows that model predictions are robust only when R is of the order of 1, which holds for all cases that we explore.

Steady states of the NSM. From the solution to the single internal fixed point (Eq. (2), see Methods), an obvious constraint on the NSM is that the reproduction rate λ must be less than the starvation rate σ, so that the consumer and resource densities are positive. The condition $\sigma = \lambda$ thus represents a transcritical (TC) bifurcation[31] that demarcates a physical from an unphysical regime where all steady-state densities become negative after intersecting the trivial fixed point $(F^*, H^*, R^*) = (0, 0, 0)$. The biological implication of the constraint $\lambda < \sigma$ has a simple interpretation—the rate at which a macroscopic organism loses mass due to lack of resources is generally much faster than the rate of reproduction. As we will discuss below, this inequality is a natural consequence of allometric constraints[3] for organisms within empirically observed body size ranges.

In the physical regime of $\lambda < \sigma$, the fixed point (2) may either be a stable node or a limit cycle (Fig. 1). In continuous-time systems, a limit cycle arises when a pair of complex conjugate eigenvalues crosses the imaginary axis to attain positive real parts[32]. This Hopf bifurcation is defined by $\mathrm{Det}(\mathbf{S}) = 0$, with $\mathbf{S}$ the Sylvester matrix, which is composed of the coefficients of the characteristic polynomial of the Jacobian matrix[33]. As the system parameters are tuned to be within the stable regime, but close to the Hopf bifurcation, the amplitude of the transient cycles becomes large. Given that ecological systems are constantly being perturbed[34], the onset of transient cycles, even though they decay with time in the mean-field description, can increase extinction risk[35–37].
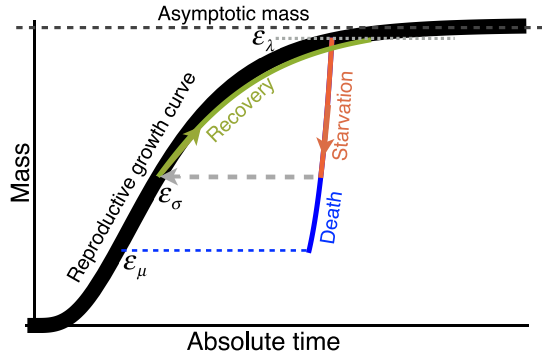
Figure 2: The growth trajectory over absolute time of an individual organism as a function of body mass. Initial growth follows the black trajectory to an energetically replete reproductive adult mass $m = \epsilon_\lambda M$. Starvation follows the red trajectory to $m = \epsilon_\sigma \epsilon_\lambda M$. Recovery follows the green curve to the replete adult mass, where this trajectory differs from the original growth because only fat is being regrown which requires a longer time to reach $\epsilon_\lambda M$. Alternatively, death from starvation follows the blue trajectory to $m = \epsilon_\mu \epsilon_\lambda M$.

When the starvation rate $\sigma \gg \lambda$, a substantial fraction of the consumers are driven to the hungry non-reproducing state. Because reproduction is inhibited, there is a low steady-state consumer density and a high steady-state resource density. However, if $\sigma/\lambda \to 1$ from above, the population is overloaded with energetically-replete (reproducing) individuals, thereby promoting transient oscillations between the consumer and resource densities (Fig. 1). If the starvation rate is low enough that the Hopf bifurcation is crossed, these oscillations become stable over time. This threshold occurs at higher values of the starvation rate as the recovery rate ρ increases, such that the range of parameter space giving rise to cyclic dynamics also increases with higher recovery rates.

Results

The allometry of extinction risk. While there are no *a priori* constraints on the parameters in the NSM, we expect that each species should be restricted to a distinct portion of the parameter space. We use allometric scaling relations to constrain the covariation of rates in a principled and biologically meaningful manner (see Methods). Allometric scaling relations highlight common constraints and average trends across large ranges in body size and species diversity. Many of these relations can be derived from a small set of assumptions and in the Methods we describe our framework to determine the covariation of timescales and rates across a range of body sizes for each of the key parameters of our model (cf. ref.[38]).

Nearly all of the rates described in the NSM are determined by consumer metabolism, which can be used to describe a variety of organismal features[39]. We derive relationships for the rates of reproduction, starvation, recovery, and mortality based on first principles, and as a function of an organism's body size and metabolic rate (see Methods). Because we aim to explore the starvation-recovery dynamics as a function of an organism's body mass M, we parameterize these rates in terms of the *percent* gain and loss of the asymptotic (maximum) body mass, ϵM, where different values of ϵ define different states of the consumer (Fig. 2; see Methods for derivations of allometrically constrained rate equations). Although the rate equations (1) are general and can in principle be used to explore the starvation recovery dynamics for most organisms, here we focus on allometric relationships for terrestrial-bound lower trophic level endotherms (see the SI for values), specifically herbivorous mammals, which range from a minimum of $M \approx 1$g (the Etruscan shrew *Suncus etruscus*) to a maximum of $M \approx 10^7$g (the early Oligocene Indricotheriinae and the Miocene Deinotheriinae). Investigating other classes of organisms would simply involve altering the metabolic exponents and scalings associate with ϵ. Moreover, we emphasize that our allometric equations describe mean relationships, and do not account for the (sometimes considerable) variance associated with individual species.

As the allometric derivations of the NSM rate laws reveal (see Methods), starvation and recovery rates are not independent parameters, and the biologically relevant portion of the phase space shown in Fig. 1 is constrained via covarying parameters. Given the parameters of terrestrial endotherms, we find that the starvation rate σ and the recovery rate ρ are constrained to lie within a small region of potential values for the known range of body sizes M. Indeed, starvation and recovery rates across all values of M fall squarely in the steady state region at some distance from the Hopf bifurcation. This suggests that cyclic population dynamics should be rare, particularly in environments where resources are limiting.

Higher rates of starvation result in a larger flux of the population to the hungry state. In this state, reproduction is absent, thus increasing the likelihood of extinction. From the perspective of population survival, it is the rate of starvation relative to the rate of recovery that determines the long-term dynamics of the various species (Fig. 1). We therefore examine the competing effects of cyclic dynamics vs. changes in steady-state density on extinction risk, both as functions of σ and ρ. To this end, we computed the probability of extinction, where we define extinction as a population trajectory falling below one fifth of the allometrically constrained steady state at any time between $t = 10^8$ and $t = 10^{10}$. This procedure is repeated for 50 replicates of the continuous-time system shown in Eq. 1 for organisms with mass ranging from 10^2 to 10^6 grams. In each replicate the initial densities are chosen to be (XF^*, XH^*, R^*), with X a random variable that is uniformly distributed in $[0, 2]$. By allowing the rate of starvation to vary, we assessed extinction risk across a range of values for σ and ρ between ca. 10^{-7} to
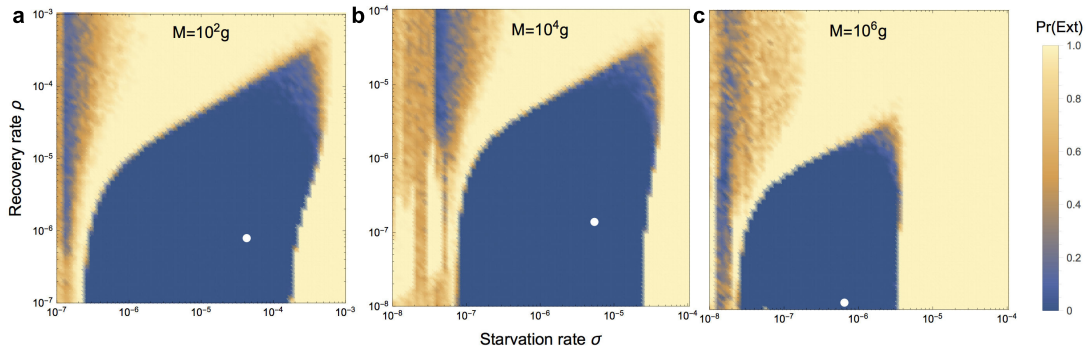
Figure 3: Probability of extinction for a consumer with (**a**) $M = 10^2$g, (**b**) $M = 10^4$g, and (**c**) $M = 10^6$g as a function of the starvation rate σ and recovery rate ρ, where the initial density is given as (XF^*, XH^*, R^*), where X is a random uniform variable in $[0, 2]$. Note the change in scale for $M = 10^4$ and $M = 10^6$g. Extinction is defined as the population trajectory falling below $0.2\times$ the allometrically constrained steady state. The white points denote the allometrically constrained starvation and recovery rate.

10^{-3}. As expected, higher rates of extinction correlate with both high values of σ if ρ is small, and high values of ρ if σ is small. For low values of σ and high values of ρ, the increased extinction risk results from transient cycles with larger amplitudes as the system nears the Hopf bifurcation (Fig. 3). For high values of σ and low values of ρ, increased extinction risk arises because of the decrease in the steady-state consumer population density (Figs. 1b, 3). This interplay creates an 'extinction refuge', such that for a constrained range of σ and ρ, extinction probabilities are minimized.

We find that the allometrically constrained values of σ and ρ fall squarely within the extinction refuge across a range of M (Fig. 3a-c, white points). These values are close enough to the Hopf bifurcation to avoid low steady-state densities, and far enough away to avoid large-amplitude transient cycles. The feature that allometric values of σ and ρ fall within this relatively small window supports the possibility that a selective mechanism has constrained the physiological conditions that drive starvation and recovery rates within populations. Such a mechanism would select for organism physiology that generates appropriate σ and ρ values that serve to minimize extinction risk. This selection could occur via the tuning of body fat percentages, metabolic rates, and biomass maintenance efficiencies. We also find that as body size increases, the amount of low extinction risk parameter space becomes smaller (Fig. 3a-c), suggesting that the population dynamics of larger organisms are more sensitive to variability in physiological rates controlling starvation and recovery. This finding is in accordance with, and may serve as contributing support for, observations of increased extinction risk among larger mammals[40]. Moreover, larger body sizes decrease the steady state resource density, such that fluctuations for larger organisms will be more likely to drive resources to extinction. To summarize, our finding that the allometrically-determined parameters fall within this low extinction probability region suggests that the NSM dynamics may both drive—and constrain—natural animal populations.

Predicting Damuth's Law and body size limits. The NSM correctly predicts that species with smaller masses have larger steady-state population densities (Fig. 4a). Similar predictions have been made for carnivore populations using alternative consumer-resource models[41]. Moreover, we show that the NSM provides independent theoretical support for Damuth's Law and the energy equivalence hypothesis[42,?,44]. Damuth's law shows that the abundances of species, N^*, follows $N^* \propto M^{-0.78}$. The energy equivalence hypothesis is based on the observation that if one assumes that the total metabolism of an ecosystem B_{tot} is equally partitioned between all species (B_i, the total metabolism of one species, is a constant), then the abundances should follow $N(M) B(M) = B_i$ implying that $N(M) \propto M^{-\eta}$, where η is the metabolic scaling exponent[43,44]. As $\eta \approx 3/4$ this hypothesis is consistent with Damuth's law[43], however the actually equivalence of energy usage of diverse species has not been measured at the population level for a variety of whole populations. Figure 4a shows that both F^* and H^* scale as $M^{-\eta}$ over a wide range of organism sizes and that $F^* + H^*$ closely matches the best fit to Damuth's data. Figure 4b shows that F^*B is nearly constant over this same range. This result is remarkable because it illustrates that the steady state values of the NSM combined with the derived timescales naturally give rise to Damuth's law. While the previous metabolic studies supporting Damuth's law provided arguments for the value of the exponent[43], these studies are only able to infer the intercept from the data. Our model predicts not only the exponent but also this intercept by explicitly including the resource dynamics and the parameters adjusting growth and consumption.

It should be noted the density relationships of individual clades follow more shallow scaling relationships than Damuth's law[?]. In the context of our model, this
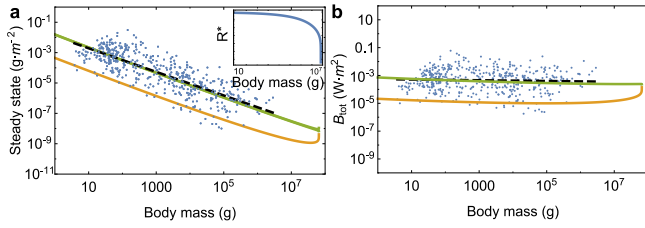
Figure 4: (**a**) Consumer steady states F^* (green) and H^* (orange) as a function of body mass. Inset: Resource steady state R^* as a function of consumer body mass. (**b**) Total energetic use B_{tot} of consumer populations at the steady state as a function of body mass. The data are from Damuth[42] and have been converted to total population metabolism using the allometric relationships for metabolic rate (see the SI and Refs.[45–47]).

suggests that future work may be able to anticipate these shifts from differences in the physiological parameters associated with each clade.

Our model shows that energetic equivalence breaks down at large M suggesting that this maximum is a hard limit where deviations outside of this range are energetically suboptimal. With respect to predicted steady state densities, the total metabolic rate of F and H becomes infinite at a finite mass, and occurs at the same scale where the steady state resources vanish (Fig. 4). This asymptotic behavior is governed by body sizes at which ϵ_μ and ϵ_λ equal zero, causing the timescales to become infinite and the rates μ and λ to equal zero. A theoretical upper bound on mammalian body size is given by $\epsilon_\sigma = 0$, where mammals are entirely composed of metabolic reserves, and this occurs at $M = 8.3 \times 10^8$ (g), or 120 times the mass of a male African elephant. In contrast, the $\mu = 0$ asymptote occurs first when $f_0 M^{\gamma-1} + u_0 M^{\zeta-1} = 1$, and corresponds to $(F^*, H^*, R^*) = (0, 0, 0)$. This point predicts a more realistic upper bound on mammalian body size and occurs at $M_{\max} = 6.54 \times 10^7$ (g). Moreover, $M_{\max}$, which is entirely determined by the population-level consequences of energetic constraints, is within an order of magnitude of the maximum body size observed in the North American mammalian fossil record[48], as well as the mass predicted from an evolutionary model of body size evolution[49]. It should be noted that the asymptotic behavior and predicted upper bound depend only on the scaling of body composition and are independent of the resource parameters. We also note that the prediction of an asymptotic limit on mammalian size parallels work on microbial life where an upper and lower bound on bacterial size, and an upper bound on single cell eukaryotic size, is predicted from similar growth and energetic scaling relationships[3,50]. It has also been shown that models of the energetic allometry of hunting and resting combined with foraging time predicts a maximum carnivore size between 7×10^5 and 1.1×10^6 (g)[60?]. Similarly, other past work has shown that the maximum body size within a particular lineage should scale with the metabolic normalization constant and depend on a critical death found to be constant from data[61]. This complementary approach is based on the balance between death and growth, and in connection with our model here suggests that future connections between the scaling of fat and muscle mass should be systematically connected with B_0 when comparing lineages.

A mechanism for Cope's rule Metabolite transport constraints are widely thought to place strict boundaries on biological scaling[39,51,52] and thereby lead to specific predictions on the minimum possible body size for organisms[53]. Above this bound, a number of energetic and evolutionary mechanisms have been explored to assess the costs and benefits associated with larger body masses, particularly for mammals. One important such example is the *fasting endurance hypothesis*, which contends that larger body size, with consequent lower metabolic rates and increased ability to maintain more endogenous energetic reserves, may buffer organisms against environmental fluctuations in resource availability[54]. Over evolutionary time, terrestrial mammalian lineages show a significant trend towards larger body size known as Cope's rule[48,49,55,56], and it is thought that within-lineage drivers generate selection towards an optimal upper bound of roughly 10^7 grams[48], a value that is likely limited by higher extinction risk for large taxa over longer timescales[49]. These trends are thought to be driven by a combination of climate change and niche availability[56]; however the underpinning energetic costs and benefits of larger body sizes, and how they influence dynamics over ecological timescales, have not been explored.

The NSM predicts that the steady state resource density R^* decreases with increasing body size of the consumer population (Fig. 4a, inset), and classic resource competition theory predicts that the species surviving on the lowest resource abundance will outcompete others[57–59]. Thus, the combined NSM steady-state dynamics and allometric timescales predict that larger mammals have an intrinsic competitive advantage given a common resource, but these absolute limits do not offer a mechanism by which larger body sizes are selected for or against.

We directly assess competitive outcome between two closely related species: a resident species of mass M, and a competing species (denoted by $'$) where individuals have a different proportion of body fat such that $M' = M(1 + \chi)$. If $\chi < 0$, individuals within the competing population have fewer metabolic reserves, and if $\chi > 0$, individuals have more metabolic reserves than the resident species. For the allowable values of χ the adjusted mass should exceed the minimal amount of body fat, $1 + \chi > \epsilon_\sigma$, and the adjusted time to reproduce must be positive, which given Equation 4, implies that $1 - \epsilon_\lambda^{1-\eta} (1 + \chi)^{1-\eta} > 0$. Together these conditions imply that $\chi \in (-f_0 M^{\gamma-1}, 1/\epsilon_\lambda - 1)$ where the upper bound approximately equals 0.05 and the lower bound is mass-dependent. The modified mass adjusts our model via
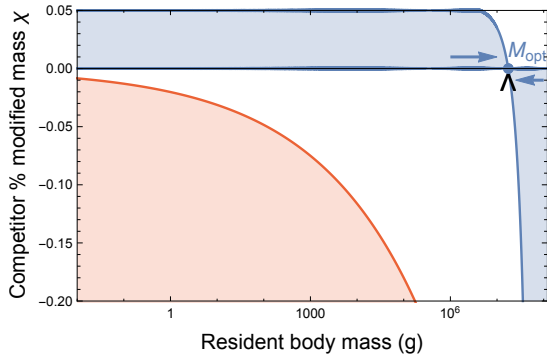
Figure 5: Competitive outcomes for a resident species with body mass M vs. a closely related competing species with modified body mass $M' = M(1 + \chi)$. The blue region denotes proportions of modified mass χ resulting in exclusion of the resident species. The red region denotes values of χ that result in a mass that is below the starvation threshold and are thus infeasible. Arrows point to the predicted optimal mass from our model $M_{\text{opt}} = 1.748 \times 10^7$, which may serve as an evolutionary attractor for body mass. The black wedge points to the largest body mass known for terrestrial mammals (*Deinotherium* spp.) at 1.74×10^7g[55].

the altered rates of starvation $\sigma(M')$, recovery $\rho(M')$, and the maintenance of both starving $\delta(M')$ and full consumers $\beta(M')$ (see the SI for detailed derivations of competitor rates). Importantly, ϵ_σ, which determines the point along the growth curve that defines the body composition of starved foragers, is assumed to remain unchanged for the competing population.

To assess the susceptibility of the resident species to competitive exclusion, we determine which consumer pushes the steady-state resource density R^* to lower values for a given value of χ, with the expectation that a population capable of surviving on lower resource densities has a competitive advantage[57]. We find that for $M \leq 1.748 \times 10^7$g, having additional body fat ($\chi > 0$) results in a lower steady state resource density ($R'^* < R^*$), such that the competitor has an intrinsic advantage over the resident species (Fig. 5). However, for $M > 1.748 \times 10^7$g, leaner individuals ($\chi < 0$) have lower resource steady state densities, switching the advantage from having more metabolic reserves to having less.

The observed switch in susceptibility as a function of χ at $M_{\text{opt}} = 1.748 \times 10^7$g thus serves as an attractor, such that the NSM predicts organismal mass to increase if $M < M_{\text{opt}}$ and decrease if $M > M_{\text{opt}}$. This value is close to but smaller than the asymptotic upper bound for terrestrial mammal body size predicted by the NSM, however it is remarkably close to independent estimates of the largest land mammals, the early Oligocene *Indricotherium* at ca. 1.5×10^7g and the late Miocene *Deinotherium* at ca. 1.74×10^7g [55]. Additionally, our calculation of M_{opt} as a function of mass-dependent physiological rates is similar to theoretical estimates of maximum body size[49], and provides independent theoretical support for the observation of a 'maximum body size

attractor' for North American mammals explored by Alroy[48]. It should be noted that the model of[51] predicts an optimal mammal size at intermediate mammalian sizes using reproductive maximization. This model considers the transition between hungry and full individuals as well, but our coupling to resources and an explicit treatment of storage shows that the largest mammals have an advantage in terms resource competition. Another subtlety is that the distributions in[51] show that intermediate mammal sizes have the most number of species, and it is important to recognize that our efforts consider total biomass where recent work shows that many ecosystems are dominated by the biomass of the large.

While the state of the environment, as well as the competitive landscape, will determine whether specific body sizes are selected for or against[56], we propose that the dynamics of starvation and recovery described in the NSM provide a general selective mechanism for the evolution of larger body size among terrestrial mammals.

Discussion

The energetics associated with somatic maintenance, growth, and reproduction are important elements that influence the dynamics of all populations[11]. The NSM is a general model that incorporates the dynamics of starvation and recovery that are expected to occur in resource-limited environments. By incorporating allometric relations between the rates in the NSM, we found: (i) allometrically-determined rates of starvation and recovery appear to minimize extinction risk, (ii) the dynamic consequences of these rates may introduce additional drivers and hard boundaries on the evolution of maximum body size, and (iii) a selective mechanism for the evolution of larger body sizes known as Cope's rule. We suggest that the NSM offers a means by which the dynamic consequences of energetic constraints can be assessed using macroscale interactions between and among species. Future efforts will involve exploring the consequences of these dynamics in a spatially explicit framework, thus incorporating elements such as movement costs and spatial heterogeneity, which may elucidate additional tradeoffs associated with the dynamics of starvation and recovery.

Methods

Analytical solution to the NSM Equation (1) has three fixed points: two trivial fixed points at $(F^*, H^*, R^*) = (0, 0, 0)$ and $(0, 0, 1)$, and one non-trivial, internal fixed point at

$$F^* = (\sigma - \lambda)\frac{\alpha\lambda\mu^2(\mu + \xi\rho)}{A(\lambda\rho B + \mu\sigma(\beta\mu + \lambda(\delta + \rho)))},$$

$$H^* = (\sigma - \lambda)\frac{\alpha\lambda^2\mu(\mu + \xi\rho)}{A(\lambda\rho B + \mu\sigma(\beta\mu + \lambda(\delta + \rho)))}, \quad (2)$$

$$R^* = (\sigma - \lambda)\frac{\mu}{A}.$$

where $A = (\lambda\xi\rho + \mu\sigma)$ and $B = (\beta\mu\xi + \delta\lambda\xi - \lambda\mu)$. The stability of this fixed point is determined by the Jacobian matrix $\mathbf{J}$, where each matrix element $J_{ij} = \partial\dot{X}_i/\partial X_j$ when evaluated at the internal fixed point, and $\mathbf{X}$ is the vector (F, H, R). The parameters in Eq. (1) are such that the real part of the largest eigenvalue of $\mathbf{J}$ is negative, so that the system is stable with respect to small perturbations from the fixed point. Because this fixed point is unique, it is the global attractor for all population trajectories for any initial condition where the resource and consumer densities are both nonzero.

Metabolic scaling relationships The scaling relation between an organism's metabolic rate B and its body mass M at reproductive maturity is known to scale as $B = B_0 M^{\eta}$[62], where the scaling exponent η is typically close to 2/3 or 3/4 for metazoans (e.g., ref.[39]), and has taxonomic shifts for unicellular species between $\eta \approx 1$ in eukaryotes and $\eta \approx 1.76$ in bacteria[3,63].

Several efforts have shown how a partitioning of B between growth and maintenance purposes can be used to derive a general equation for both the growth trajectories and growth rates of organisms ranging from bacteria to metazoans[3,45-47,64]. This relation is derived from the simple balance condition $B_0 m^{\eta} = E_m \dot{m} + B_m m$,[3,45-47,64] where E_m is the energy needed to synthesize a unit of mass, B_m is the metabolic rate to support an existing unit of mass, and m is the mass of the organism at any point in its development. This balance has the general solution[3,65]

$$\left(\frac{m(t)}{M}\right)^{1-\eta} = 1 - \left[1 - \left(\frac{m_0}{M}\right)^{1-\eta}\right] e^{-a(1-\eta)t/M^{1-\eta}}, \quad (3)$$

where, for $\eta < 1$, $M = (B_0/B_m)^{1/(1-\eta)}$ is the asymptotic mass, $a = B_0/E_m$, and m_0 is mass at birth, itself varying allometrically (see the SI). We now use this solution to define the timescale for reproduction and recovery from starvation (Fig. 2; see[47] for a detailed presentation of these timescales). The time that it takes to reach a particular mass ϵM is given by the timescale

$$\tau(\epsilon) = \ln\left[\frac{1 - (m_0/M)^{1-\eta}}{1 - \epsilon^{1-\eta}}\right] \frac{M^{1-\eta}}{a(1-\eta)}, \quad (4)$$

where we will define values of ϵ to describe a variety of timescales, and related rates, within our model. For example, the rate of reproduction is given by the timescale to go from the birth mass to the adult mass. The time to reproduce is given by Equation 4 as $t_{\lambda} = \tau(\epsilon_{\lambda})$, where ϵ_{λ} is the fraction of the asymptotic mass where an organism is reproductively mature and should be close to one (typically $\epsilon_{\lambda} \approx 0.95$ [45]). Our reproductive rate, λ, is a specific rate, or the number of offspring produced per time per individual, defined as $\dot{F} = \lambda F$. In isolation this functional form gives population growth following $F(t) = F_0 e^{\lambda t}$ which can be related to the reproductive timescale by assuming that when $t = t_{\lambda}$ it is also the case that $F = \nu F_0$, where $\nu - 1$ is the number of offspring produced per reproductive cycle. Following this relationship the growth rate is given by $\lambda = \ln(\nu)/t_{\lambda}$, which is the standard relationship and will scale as $\lambda \propto M^{\eta-1}$ for $M \gg m_0$ for any constant value of ϵ_{λ}[3,45-47,64].

The rate of recovery $\rho = 1/t_{\rho}$ requires that an organism accrues sufficient tissue to transition from the hungry to the full state. Since only certain tissues can be digested for energy (for example the brain cannot be degraded to fuel metabolism), we define the rates for starvation, death, and recovery by the timescales required to reach, or return from, specific fractions of the replete-state mass (see the SI, Table I, for parameterizations). We define $m_{\sigma} = \epsilon_{\sigma} M$, where $\epsilon_{\sigma} < 1$ is the fraction of replete-state mass where reproduction ceases. This fraction will deviate from a constant if tissue composition systematically scales with adult mass. For example, making use of the observation that body fat in mammals scales with overall body size according to $M_{\text{fat}} = f_0 M^{\gamma}$ and assuming that once this mass is fully digested the organism starves, this would imply that $\epsilon_{\sigma} = 1 - f_0 M^{\gamma}/M$. It follows that the recovery timescale, t_{ρ}, is the time to go from $m = \epsilon_{\sigma}\epsilon_{\lambda} M$ to $m = \epsilon_{\lambda} M$ (Fig. 2). Using Eqs. (3) and (4) this timescale is given by simply considering an adjusted starting mass of $m_0' = \epsilon_{\sigma}\epsilon_{\lambda} M$, in which case

$$t_{\rho} = \ln\left[\frac{1 - (\epsilon_{\sigma}\epsilon_{\lambda})^{1-\eta}}{1 - \epsilon_{\lambda}^{1-\eta}}\right] \frac{M^{1-\eta}}{a'(1-\eta)} \quad (5)$$

where $a' = B_0/E_m'$ accounts for possible deviations in the biosynthetic energetics during recovery (see the SI). It should be noted that more complicated ontogenetic models explicitly handle storage[46], whereas this feature is implicitly covered by the body fat scaling in our framework.

To determine the starvation rate, σ, we are interested in the time required for an organism to go from a mature adult that reproduces at rate λ, to a reduced-mass hungry state where reproduction is impossible. For starving individuals we assume that an organism must meet its maintenance requirements by using the digestion of existing mass as the sole energy source. This assumption implies the following simple metabolic balance $\dot{m}E_m' = -B_m m$ or $\dot{m} = -a'm/M^{1-\eta}$ where E_m' is the amount of energy stored in a unit of existing body mass, which differs from E_m, the energy required to synthesis a unit of biomass[46]. Given the replete mass, M, of an organism, the above energy balance prescribes the mass trajectory of a non-consuming organism: $m(t) = Me^{-a't/M^{1-\eta}}$. The timescale for starvation is given by the time it takes $m(t)$ to reach $\epsilon_{\sigma} M$, which gives

$$t_{\sigma} = -\frac{M^{1-\eta}}{a'} \ln(\epsilon_{\sigma}). \quad (6)$$

The starvation rate is then $\sigma = 1/t_{\sigma}$, which scales with replete-state mass as $1/M^{1-\eta} \ln(1 - f_0 M^{\gamma}/M)$. An important feature is that σ does not have a simple scaling dependence on λ, which is important for the dynamics that we later discuss.

The time to death should follow a similar relation, but defined by a lower fraction of replete-state mass, $m_{\mu} = \epsilon_{\mu} M$ where $\epsilon_{\mu} < \epsilon_{\sigma}$. Suppose, for example, that an organism dies once it has digested all fat and muscle tissues, and that muscle tissue scales with body mass according to $M_{\text{musc}} = u_0 M^{\zeta}$. This gives $\epsilon_{\mu} = 1 - (f_0 M^{\gamma} + u_0 M^{\zeta})/M$. Muscle mass has been shown to be roughly proportional to body mass[66] in mammals and thus ϵ_{μ} is merely ϵ_{σ} minus a constant. The time to go from starvation to death is the total time to reach $\epsilon_{\mu} M$ minus the time to starve, or $t_{\mu} = -M^{1-\eta} \ln(\epsilon_{\mu})/a' - t_{\sigma}$, and $\mu = 1/t_{\mu}$.

[1] Martin, T. E. Food as a limit on breeding birds: A life-history perspective. *Annu. Rev. Ecol. Syst.* **18**, 453–487 (1987).

[2] Kirk, K. L. Life-history responses to variable environments: Starvation and reproduction in planktonic rotifers. *Ecology* **78**, 434–441 (1997).

[3] Kempes, C. P., Dutkiewicz, S. & Follows, M. J. Growth, metabolic partitioning, and the size of microorganisms. *Proc. Natl. Acad. Sci. USA* **109**, 495–500 (2012).

[4] Mangel, M. & Clark, C. W. *Dynamic Modeling in Behavioral Ecology* (Princeton University Press, Princeton, 1988).

[5] Mangel, M. Stochastic dynamic programming illuminates the link between environment, physiology, and evolution. *B. Math. Biol.* **77**, 857–877 (2014).

[6] Yeakel, J. D., Dominy, N. J., Koch, P. L. & Mangel, M. Functional morphology, stable isotopes, and human evolution: a model of consilience. *Evolution* **68**, 190–203 (2014).

[7] Morris, D. W. Optimal allocation of parental investment. *Oikos* **49**, 332–339 (1987).

[8] Tveraa, T., Fauchald, P., Henaug, C. & Yoccoz, N. G. An examination of a compensatory relationship between food limitation and predation in semi-domestic reindeer. *Oecologia* **137**, 370–376 (2003).

[9] Daan, S., Dijkstra, C., Drent, R. & Meijer, T. Food supply and the annual timing of avian reproduction. In Ouellet, H. (ed.) *Acta XIX Congressus Internationalis Ornithologici, Volume I: Proceedings XIX International Ornithological Congress, 1986, Ottawa*, 392–407 (Proceedings XIX International Ornithological Congress, Ottawa, 1989).

[10] Jacot, A., Valcu, M., van Oers, K. & Kempenaers, B. Experimental nest site limitation affects reproductive strategies and parental investment in a hole-nesting passerine. *Animal Behaviour* **77**, 1075–1083 (2009).

[11] Stearns, S. C. Trade-offs in life-history evolution. *Funct. Ecol.* **3**, 259 (1989).

[12] Barboza, P. & Jorde, D. Intermittent fasting during winter and spring affects body composition and reproduction of a migratory duck. *J Comp Physiol B* **172**, 419–434 (2002).

[13] Threlkeld, S. T. Starvation and the size structure of zooplankton communities. *Freshwater Biol.* **6**, 489–496 (1976).

[14] Weber, T. P., Ens, B. J. & Houston, A. I. Optimal avian migration: A dynamic model of fuel stores and site use. *Evolutionary Ecology* **12**, 377–401 (1998).

[15] Mduma, S. A. R., Sinclair, A. R. E. & Hilborn, R. Food regulates the Serengeti wildebeest: a 40-year record. *J. Anim. Ecol.* **68**, 1101–1122 (1999).

[16] Moore, J. W., Yeakel, J. D., Peard, D., Lough, J. & Beere, M. Life-history diversity and its importance to population stability and persistence of a migratory fish: steelhead in two large North American watersheds. *J. Anim. Ecol.* **83**, 1035–1046 (2014).

[17] Mead, R. A. The Physiology and Evolution of Delayed Implantation in Carnivores. In Gittleman, J. L. (ed.) *Carnivore Behavior, Ecology, and Evolution*, 437–464 (Springer US, Ithaca, 1989).

[18] Sandell, M. The evolution of seasonal delayed implantation. *Q Rev Biol* **65**, 23–42 (1990).

[19] Bulik, C. M. *et al.* Fertility and reproduction in women with anorexia nervosa. *J. Clin. Psychiat.* **60**, 130–135 (1999).

[20] Trites, A. W. & Donnelly, C. P. The decline of Steller sea lions Eumetopias jubatus in Alaska: a review of the nutritional stress hypothesis. *Mammal Rev.* **33**, 3–28 (2003).

[21] Glazier, D. S. Metabolic level and size scaling of rates of respiration and growth in unicellular organisms. *Funct. Ecol.* **23**, 963–968 (2009).

[22] Kooijman, S. A. L. M. *Dynamic Energy and Mass Budgets in Biological Systems* (Cambridge, 2000).

[23] Sousa, T., Domingos, T., Poggiale, J. C. & Kooijman, S. A. L. M. Dynamic energy budget theory restores coherence in biology. *Philos. T. Roy. Soc. B* **365**, 3413–3428 (2010).

[24] Diekmann, O. & Metz, J. A. J. How to lift a model for individual behaviour to the population level? *Philos. T. Roy. Soc. B* **365**, 3523–3530 (2010).

[25] Murdoch, W. W., Briggs, C. J. & Nisbet, R. M. *Consumer-resource Dynamics*, vol. 36 of *Monographs in population biology* (Princeton University Press, Princeton, 2003).

[26] Benichou, O. & Redner, S. Depletion-Controlled Starvation of a Diffusing Forager. *arXiv* 1–5 (2014). 1405.5054v3.

[27] Bénichou, O., Chupeau, M. & Redner, S. Role of depletion on the dynamics of a diffusing forager. *Journal of Physics A: . . .* (2016).

[28] Chupeau, M., Bénichou, O. & Redner, S. Universality classes of foraging with resource renewal. *Phys. Rev. E* **93**, 032403 (2016).

[29] Persson, L., Leonardsson, K., De Roos, A. M., Gyllenberg, M. & Christensen, B. Ontogenetic scaling of foraging rates and the dynamics of a size-structured consumer-resource model. *Theor Popul Biol* **54**, 270–293 (1998).

[30] Murray, J. D. *Mathematical Biology: I. An Introduction*, vol. 110 of *Interdisciplinary Applied Mathematics* (Springer New York, 2011).

[31] Strogatz, S. H. *Nonlinear Dynamics and Chaos: With Applications to Physics, Biology, Chemistry, and Engineering.* Studies in nonlinearity (Westview Press, Boulder, 2008).

[32] Guckenheimer, J. & Holmes, P. *Nonlinear Oscillations, Dynamical Systems, and Bifurcations of Vector Fields* (Springer, New York, 1983).

[33] Gross, T. & Feudel, U. Analytical search for bifurcation surfaces in parameter space. *Physica D* **195**, 292–302 (2004).

[34] Hastings, A. Transient dynamics and persistence of ecological systems. *Ecol. Lett.* **4**, 215–220 (2001).

[35] Neubert, M. & Caswell, H. Alternatives to resilience for measuring the responses of ecological systems to perturbations. *Ecology* **78**, 653–665 (1997).

[36] Caswell, H. & Neubert, M. G. Reactivity and transient dynamics of discrete-time ecological systems. *J Differ Equ Appl* **11**, 295–310 (2005).

[37] Neubert, M. & Caswell, H. Detecting reactivity. *Ecology* **90**, 2683–2688 (2009).

[38] Yodzis, P. & Innes, S. Body size and consumer-resource dynamics. *Am. Nat.* **139**, 1151–1175 (1992).

[39] Brown, J., Gillooly, J., Allen, A., Savage, V. & West, G. Toward a metabolic theory of ecology. *Ecology* **85**, 1771–1789 (2004).

[40] Liow, L. H. *et al.* Higher origination and extinction rates in larger mammals. *Proc. Natl. Acad. Sci. USA* **105**, 6097–6102 (2008).

[41] DeLong, J. P. & Vasseur, D. A. A dynamic explanation of size–density scaling in carnivores. *Ecology* **93**, 470–476 (2012).

[42] Damuth, J. Interspecific allometry of population density in mammals and other animals: the independence of body mass and population energy-use. *Biol. J. Linn. Soc.* **31**, 193–246 (1987).

[43] Allen, A. P., Brown, J. H. & Gillooly, J. F. Global biodiversity, biochemical kinetics, and the energetic-equivalence rule. *Science* **297**, 1545–1548 (2002).

[44] Enquist, B. J., Brown, J. H. & West, G. B. Allometric scaling of plant energetics and population density. *Nature* **395**, 163–165 (1998).

[45] West, G. B., Brown, J. H. & Enquist, B. J. A general model for ontogenetic growth. *Nature* **413**, 628–631 (2001).

[46] Hou, C. *et al.* Energy uptake and allocation during ontogeny. *Science* **322**, 736–739 (2008).

[47] Moses, M. E. *et al.* Revisiting a Model of Ontogenetic Growth: Estimating Model Parameters from Theory and Data. *Am. Nat.* **171**, 632–645 (2008).

[48] Alroy, J. Cope's rule and the dynamics of body mass evolution in North American fossil mammals. *Science* **280**, 731–734 (1998).

[49] Clauset, A. & Redner, S. Evolutionary model of species body mass diversification. *Phys. Rev. Lett.* **102**, 038103 (2009).

[50] Kempes, C. P., Wang, L., Amend, J. P., Doyle, J. & Hoehler, T. Evolutionary tradeoffs in cellular composition across diverse bacteria. *ISME J* **10**, 2145–2157 (2016).

[51] Brown, J., Marquet, P. & Taper, M. Evolution of body size: consequences of an energetic definition of fitness. *Am. Nat.* **142**, 573–584 (1993).

[52] West, G. B., Brown, J. H. & Enquist, B. J. A general model for the origin of allometric scaling laws in biology. *Science* **276**, 122–126 (1997).

[53] West, G. B., Woodruff, W. H. & Brown, J. H. Allometric scaling of metabolic rate from molecules and mitochon-dria to cells and mammals. *Proc. Natl. Acad. Sci. USA* **99 Suppl 1**, 2473–2478 (2002).

[54] Millar, J. & Hickling, G. Fasting endurance and the evolution of mammalian body size. *Funct. Ecol.* **4**, 5–12 (1990).

[55] Smith, F. A. *et al.* The evolution of maximum body size of terrestrial mammals. *Science* **330**, 1216–1219 (2010).

[56] Saarinen, J. J. *et al.* Patterns of maximum body size evolution in Cenozoic land mammals: Eco-evolutionary processes and abiotic forcing. *Proc Biol Sci* **281**, 20132049 (2014).

[57] Tilman, D. Tests of resource competition theory using four species of lake michigan algae. *Ecology* **62**, 802–815 (1981).

[58] Dutkiewicz, S., Follows, M. J. & Bragg, J. G. Modeling the coupling of ocean ecology and biogeochemistry. *Global Biogeochem. Cycles* **23**, 1–15 (2009).

[59] Barton, A. D., Dutkiewicz, S., Flierl, G., Bragg, J. & Follows, M. J. Patterns of diversity in marine phytoplankton. *Science* **327**, 1509–1511 (2010).

[60] Carbone, C., Mace, G. M., Roberts, S. C. & Macdonald, D. W. Energetic constraints on the diet of terrestrial carnivores. *Nature* **402**, 286–288 (1999).

[61] Okie, J. G. *et al.* Effects of allometry, productivity and lifestyle on rates and limits of body size evolution. *Proc Biol Sci* **280**, 20131007–20131007 (2013).

[62] West, G. B., Woodruff, W. H. & Brown, J. H. Allometric scaling of metabolic rate from molecules and mitochondria to cells and mammals. *Proc. Natl. Acad. Sci. USA* **99 Suppl 1**, 2473–2478 (2002).

[63] DeLong, J. P., Okie, J. G., Moses, M. E., Sibly, R. M. & Brown, J. H. Shifts in metabolic scaling, production, and efficiency across major evolutionary transitions of life. *Proc. Natl. Acad. Sci. USA* **107**, 12941–12945 (2010).

[64] Gillooly, J. F., Charnov, E. L., West, G. B., Savage, V. M. & Brown, J. H. Effects of size and temperature on developmental time. *Nature* **417**, 70–73 (2002).

[65] Bettencourt, L. M. A., Lobo, J., Helbing, D., Kuhnert, C. & West, G. B. Growth, innovation, scaling, and the pace of life in cities. *Proc. Natl. Acad. Sci. USA* **104**, 7301–7306 (2007).

[66] Folland, J. P., Mc Cauley, T. M. & Williams, A. G. Allometric scaling of strength measurements to body size. *Eur J Appl Physiol* **102**, 739–745 (2008).